Do Nanotubes Follow an Amorphisation Trajectory as Other Nanocarbons Do?

Saveria Santangelo,*,§ and Candida Milone#

§ Dipartimento di Ingegneria Civile, dell'Energia, dell'Ambiente e dei Materiali (DICEAM), Università "Mediterranea", Loc. Feo di Vito, 89122 Reggio Calabria, Italy; # Dipartimento di Ingegneria Eletronica, Chimica ed Ingegneria Industriale (DIECII), Università di Messina, Viale Ferdinando Stagno d'Alcontres 31, 98166 Messina, Italy.

Supporting information

Table S1. Considered MWNTs.

Sample code	Ref.	Catalyst preparation				Synthesis reaction				Results	
		Support material	w_L (wt%)	T_C (°C)	T_R (°C)	t_S (h)	T_S (°C)	$\Phi_{i\text{-}C4H10}$ (cc/min)	Φ_{H2} (cc/min)	w_{AC} (wt%)	w_M (wt%)
L1	11	Al_2O_3	17	750	500	2.00	600	60	60	3.0	8.0
L2	11	Al_2O_3	17	750	600	2.00	600	60	60	1.2	18.3
L3	11	Al_2O_3	15	450	500	2.00	600	60	60	2.9	12.2
L4	11	Al_2O_3	15	450	500	2.00	700	60	60	0.4	4.5
L13	11	Al_2O_3	20	500	500	1.75	750	60	60	0.0	17.8
L14	15	Al_2O_3	29	500	500	2.00	600	60	60	0.0	3.5
L15	15	Al_2O_3	29	750	700	2.00	600	60	60	0.0	7.3
L16	15	Al_2O_3	29	750	700	2.00	600	90	30	0.0	15.2
L17	15	Al_2O_3	29	750	700	2.00	600	60	30	0.0	11.2
L5	15	CaO	17	750	500	2.00	600	60	60	5.1	1.3
L6	15	CaO	17	750	600	2.00	600	60	60	2.8	4.7
L7	15	CaO	15	450	500	2.00	600	60	60	4.2	4.6
L8	15	CaO	15	450	500	2.00	700	60	60	4.9	2.0
L18	11	K10/Na^+	5	500	500	2.00	700	60	60	0.0	4.2
L19	11	K10/Na^+	15	500	500	2.00	700	60	60	0.0	11.1
L20	11	K10	15	500	700	2.00	700	60	60	0.0	10.4
L9	15	MgO	17	750	500	2.00	600	60	60	4.8	1.6
L10	15	MgO	17	750	600	2.00	600	60	60	2.8	1.0
L11	15	MgO	15	450	500	2.00	600	60	60	3.6	1.3
L12	15	MgO	15	450	500	2.00	700	60	60	3.1	1.9
		Diameter range (nm)									
P1		<10								0.0	0.3
P2	11	5−20								0.0	3.3
P3	11	10−30								0.0	6.7
P4	11	40−60								0.0	4.1
P5	11	60−100								0.0	3.7
		Pristine sample				Annealing temperature (°C)					
A1		L14				1000				0.0	2.7
A2		L15				1000				0.0	1.7
A3		L14				1500				0.0	2.7
A4		L15				1500				0.0	1.7

Laboratory prepared, purchased and annealed MWNTs are respectively coded as "L", "P" and "A". Synthesis conditions, diameter ranges and annealing temperature are reported for the three types of samples, respectively. In case of laboratory prepared MWNTs, T_C and T_R are calcination- and reduction-temperatures of the catalysts; w_L denotes loaded iron by impregnation, which in montmorillonite-supported catalysts adds up to iron contained in the support (2.0 wt.% in K10- and 1.7 wt.% in K10/ Na^+-montmorillonite, respectively); t_S and T_S are duration and temperature of the synthesis reactions, carried over 500 mg of catalyst, excepted sample L13, for which 1000 mg were used; $\Phi_{i\text{-}C4H10}$ and Φ_{H2} are the reactive gas flow rates (for sample L17 the total flow is kept at 120 cc/min by using He as a balance-gas). w_{AC} and w_M stand respectively for the relative contents of amorphous carbon and metallic impurities, as inferred from thermo-gravimetry.

(11) Santangelo S.; Messina G.; Faggio G.; Lanza M.; Milone C., Evaluation of Crystalline Perfection Degree of Multi-Walled Carbon Nanotubes: Correlations between Thermal Kinetic Analysis and Micro-Raman Spectroscopy. *J. Raman Spectr.* **2011**, *42*, 593−602.

(15) Santangelo S.; Lanza M.; Milone C., Evaluation of the Overall Crystalline Quality of Amorphous Carbon Containing Multi-Walled Carbon Nanotubes. *J. Phys. Chem. C.* **2013**, *117*, 4815−4823.

Growth and Preliminary Characterization

A detailed description of catalyst preparation, growth experiments, subsequent sample purification and preliminary characterization, together with an extensive discussion concerning the influence of CVD parameters on the resulting MWNT specifics, can be found in [a,b,c,d] and refs cited therein.

The mass percent of non-burnt matter at the end of each thermo-gravimetry analysis gives the relative content of encapsulated metal-nanoparticles (w_M).[c,d] The mass losses in the 200–400 °C and 400–600 °C temperature ranges of the thermograms, where the combustion of amorphous/disordered and ordered carbonaceous species takes place give the relative contents of amorphous carbon (w_{AC}) and NTs (w_{NT}). Of course, $w_{AC}+w_M+w_{NT}=100$wt%.

The purity degree (w_C) of each sample is defined as complement to 100 of w_M, $w_C=100-w_M$.

The amorphous fraction (f_{AC}) is given by $100 \cdot w_{AC}/w_C$.

(a) Messina G.; Modafferi V.; Santangelo S.; Tripodi P.; Donato M.G.; Lanza M.; Galvagno S.; Milone C.; Piperopoulos E.; Pistone A., Large-scale production of high-quality multi-walled carbon nanotubes: role of precursor gas and of Fe-catalyst support. *Diam. Rel. Mater.* **2008**, *17*, 1482–1488.

(b) Donato M.G.; Faggio G.,; Galvagno S.; Lanza M.; Messina G.; Milone C.; Piperopoulos E.; Pistone A.; Santangelo S., Influence of gas-mixture composition on yield, purity and morphology of C nanotubes grown by catalytic isobutane-decomposition *Diam. Rel. Mater.* **2009**, *18*, 360–363.

(c) Santangelo S.; Dhanagopal M.; Faggio G.; Messina G.;, Pistone A.; Lanza M.; Milone C., Preparation of nanotubes-clay hybrid systems by iron-catalyzed isobutane decomposition *Diam. Rel. Mater.* **2010**, *19*, 599–604.

(d) Santangelo S.; Piperopoulos E.; Lanza M.; Milone C., Growth and Analysis of C Nanotubes on Ceramic Polymer-Additives. *J. Nanosci. Nanotechnol.* **2012**, *12*, 4786–4797.

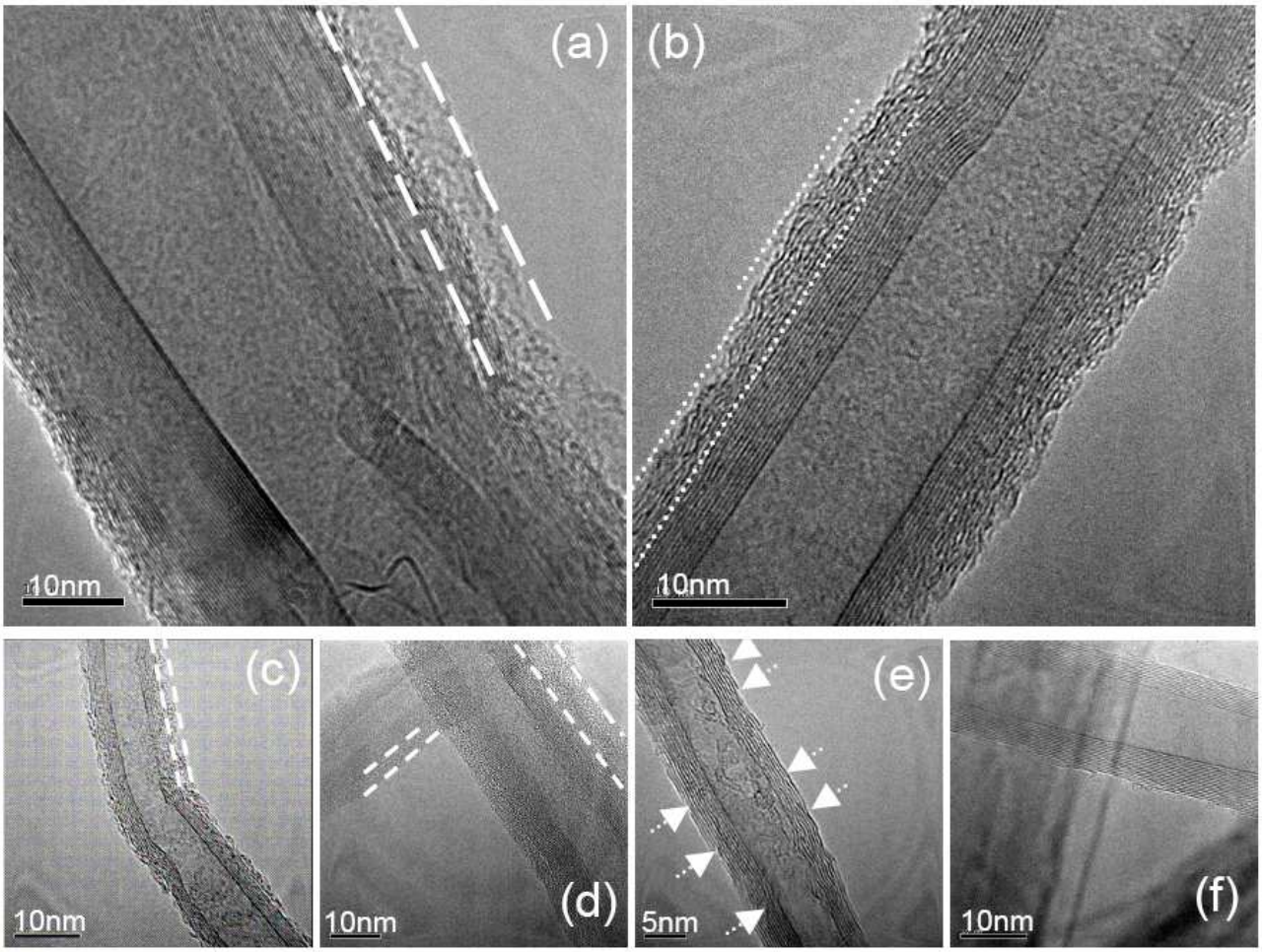

Figure S1. Representative HRTEM images of AC-containing (a–e) and AC-free (f) MWNTs. Shown nanographs refer to samples L8 (a,b), L3 (c), L9 (d,e) and L18 (f). Images (b) and (e) are taken after oxidation at 220 °C for 1 h. In images (a), (c) and (d) dashed lines highligth the thick amorphous layer externally coating the tubes; in images (b) and (e) dotted lines and arrows respectively highligth AC coating survived to oxidation and interconnections between undulated graphene layers.

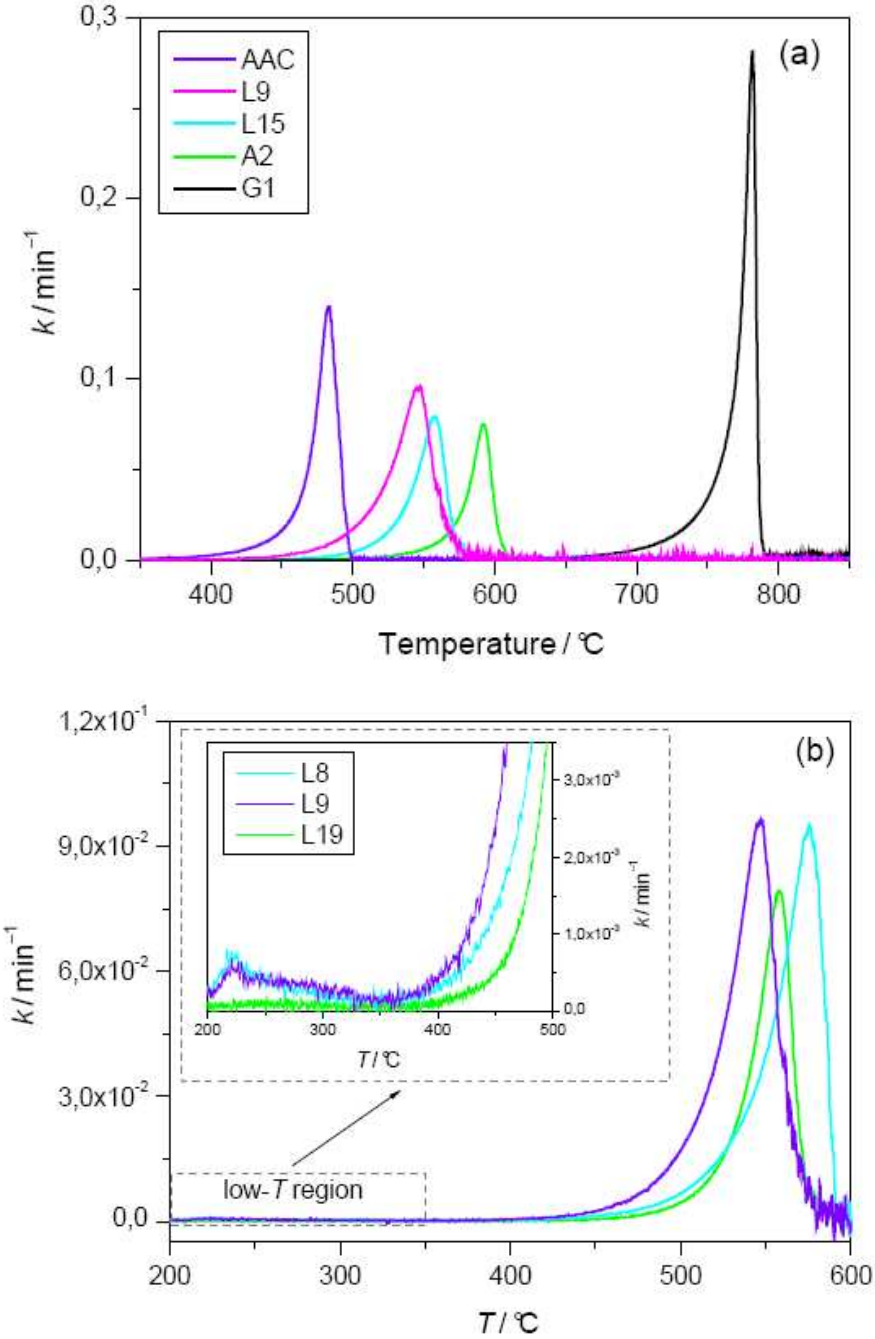

Figure S2. (a) Typical kinetic oxidation profiles of investigated samples. (b) Comparison between kinetic oxidation profiles of AC-containing and AC-free MWNTs (inset: low-T regions of profiles).

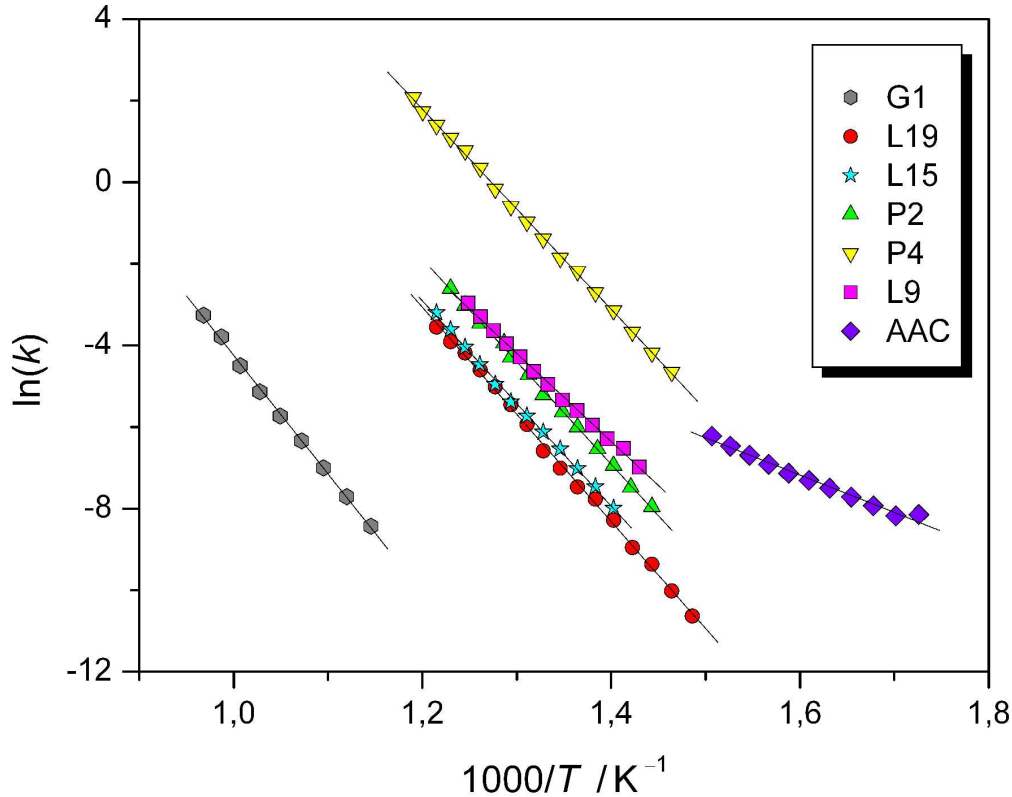

Figure S3. Arrhenius plots of oxidation rate constants (k) for some representative samples.

Kinetic approach to the study of oxidation

The rate constant (k) for a heterogeneous reaction of the type (Solid) + (Gas) → (Gas), as carbon oxidation, is usually expressed as

$$k(T) = -(1/m)\cdot \mathrm{d}m/\mathrm{d}t\,, \qquad (1)$$

where m is the instantaneous mass of carbon,[e] t is the time, and T is the instantaneous absolute temperature that increases linearly with t.

According to this kinetic model, if concentration of the gaseous reactant is constant and in large excess with respect to that of carbon (as here ensured by the experimental conditions), reaction order is one with respect to carbon and zero with respect to the gaseous reactant.[f] Eqn (1) can be thus rewritten as

$$k(T) = A\cdot \mathrm{e}^{-E_A/RT}, \qquad (2)$$

with A the frequency factor, E_A the activation energy and R is the universal gas constant, i.e. the kinetic rate for carbon oxidation follows the Arrhenius equation. Hence, the apparent activation energy for oxidation of the carbonaceous material can calculated from the slope of the Arrhenius plot of its kinetic oxidation profile.

For further details see ref 11 and refs therein cited.

(11) Santangelo S.; Messina G.; Faggio G.; Lanza M.; Milone C., Evaluation of Crystalline Perfection Degree of Multi-Walled Carbon Nanotubes: Correlations between Thermal Kinetic Analysis and Micro-Raman Spectroscopy. *J. Raman Spectr.* **2011**, *42*, 593−602.

(e) Zaghib K.; Song X.; Kinoshita K., *Termochim. Acta* **2001**; *371*, 57–64.

(f) Wunderlich B., *Thermal characterization of polymeric materials*, (Ed.: E.A. Turi), Accademic Press Inc., San Diego, **1981**, p. 112.

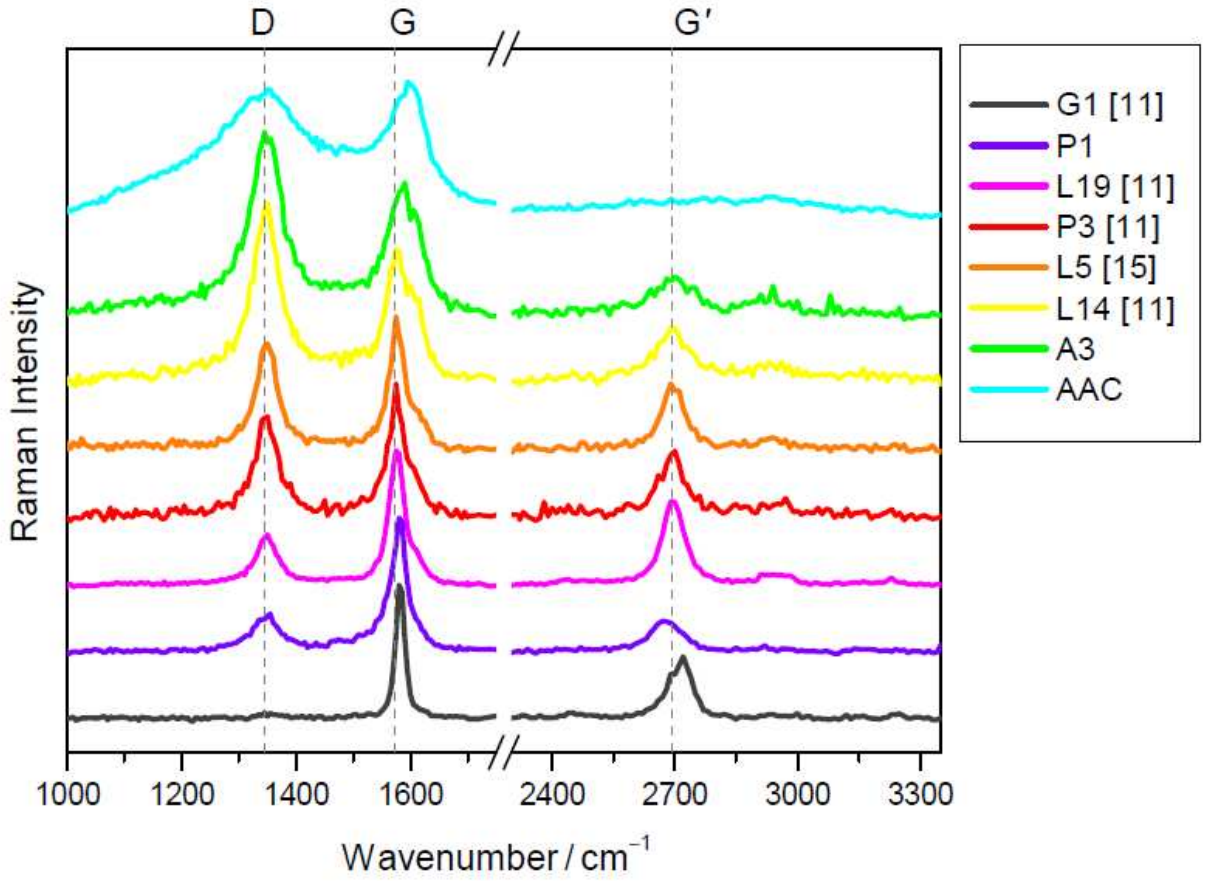

Figure S4. Micro-Raman spectra of the most representative samples. Spectra are normalized to the G-band intensity for an easier comparison.

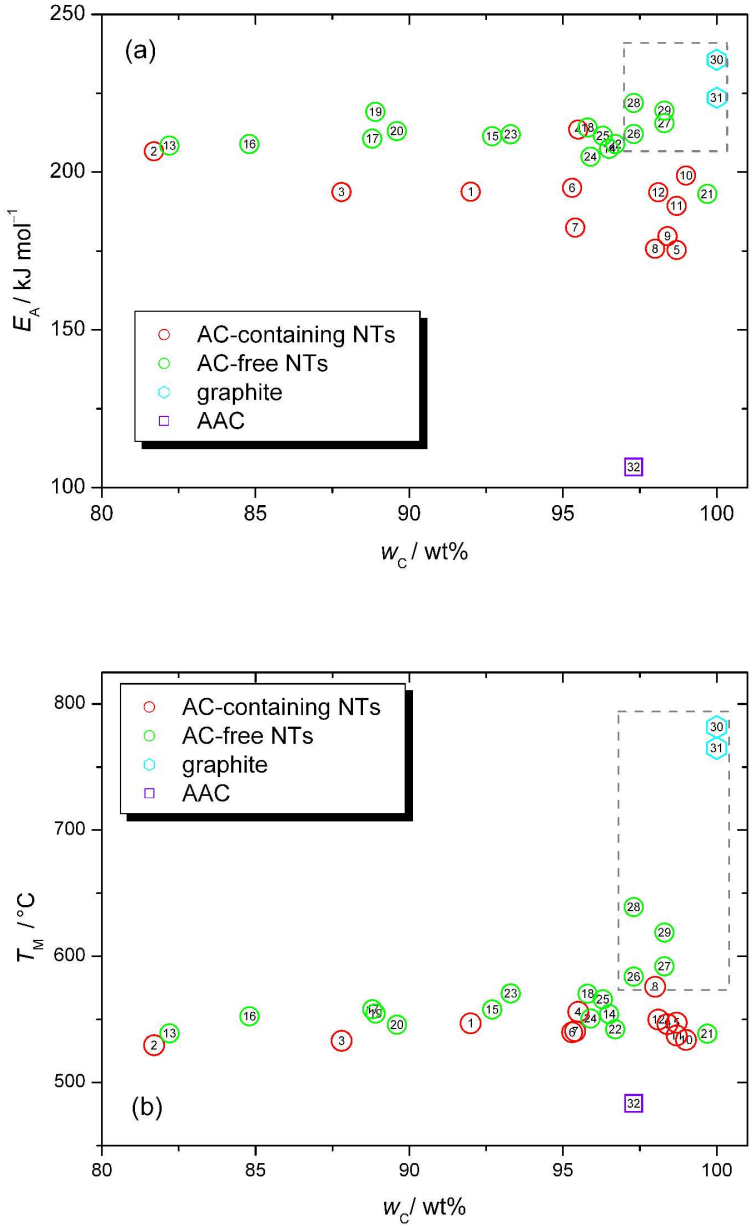

Figure S5. Dependence on purity degree (w_C) of (a) the apparent activation energy (E_A) for the oxidation and (b) maximum oxidation rate temperature (T_M).

Role of the metallic impurities

Plotting apparent activation energy (E_A) and maximum oxidation rate temperature (T_M) relative to all the entries of Table 1 as a function of the sample purity degree (w_C=100–w_M) proves that the concentration of metal-nanoparticles (w_M), here passivated by coke, plays no definite role on reactivity and thermal stability of the samples, different from what reported for NTs decorated with metal and metal oxides nanoparticles.[30] On the contrary, the behavior of graphite and annealed NTs (within the dashed box) demonstrates that improved crystalline perfection and graphitic ordering are mainly responsible for reactivity lowering and oxidative resistance.

(30) Leino A.R.; Mohl M.; Kukkola J.; Mäki-Arvela P.; Kokkonen T.; Shchukarev A.; Kordas K., Low-Temperature Catalytic Oxidation of Multi-Walled Carbon Nanotubes. *Carbon* **2013**, 57, 99–107.

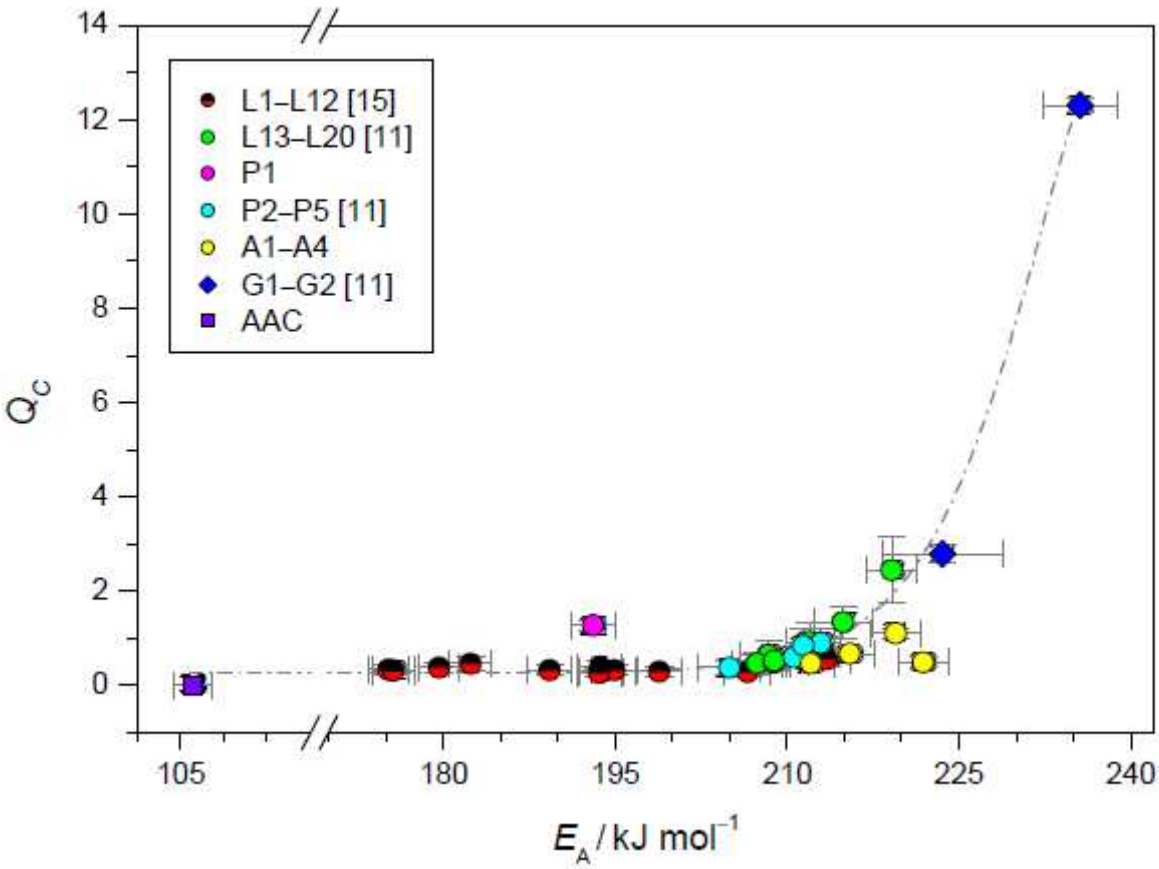

Figure S6. Raman descriptor (Q_C) of the overall crystalline quality of considered nanocarbons as a function of the apparent activation energy for their oxidation (E_A) inferred from KTA. Dash-dotted line represents the best fit to data.

Note that in highly reactive samples (E_A < 200 kJ/mol) Q_C is consistently low, but insensitive to the variation of E_A. Thus, it cannot accounts for further reactivity enhancements (E_A decrease). Instead, as previously demonstrated for AC-containing MWNTs,[15] E_A is sensitive to the variations of amorphous fraction, as assessed through TG: it undergoes a coarsely linear decrease with f_{AC} increasing in the range 0.4−5.2 wt% (see lower f_{AC} side of Figure S5a). The correlation still holds when the f_{AC} variation range is extended up to 100.0 wt% to include AAC. In such case, the activation energy for oxidation is found to decline exponentially with a power (1.7) of the amorphous fraction (Figure S7a). Moreover, this function more accurately fits to the data of AC-containing MWNTs (see inset of Figure S7a). This indicates that surface properties of these samples well correlate with kinetics of their oxidation. This is true also for AC-free samples.

Studying pristine, chemically oxidized and heat treated MWNTs with different outer diameters (15−160 nm), Delhaes et al.[10] demonstrated the existence of a correlation between the in-plane coherence length, as deduced from Raman scattering measurements (i.e. L_C), and the global active surface area (ASA), giving a measure of the density of oxygenated functional groups (that are present on the surface of pristine samples too[10,19]).

In the relationship that they derived,

$$\log(\mathrm{ASA}) = 2.3 - 1.7\log(L_C) \qquad (2)$$

ASA, expressed in m^2/g, tends to the limiting value of ~200 m^2/g for a supposed value of L_C = 1 nm.

ASA values relative to present pristine AC-free MWNTs (with outer diameter > 10 nm) were estimated inserting in eq (2) L_C values reported in Table 1. Figure S7b shows a semi-logarithmic plot of E_A against results obtained

for ASA. E_A is found to decrease linearly with increasing log(ASA), i.e. with the density of surface functional groups as indirectly estimated through MRS. Such dependence still holds when representative points relative to graphite are included (lower ASA side of Figure S7b), indicating that in absence of AC and marked sp^3 hybridization of C bonds (arising from high curvature of and/or large disorder within the graphene layers), nanocarbons behave similarly independently on the fact that they are formed by flat piled or cylindrical rolled up graphene layers.

(10) Delhaes P.; Couzi M.; Trinquecoste M.; Dentzer J., Hamidou H.; Vix-Guterl C., A Comparison between Raman Spectroscopy and Surface Characterizations of Multiwall Carbon Nanotubes. Carbon **2006**, *44*, 3005–3013.

(15) Santangelo S.; Lanza M.; Milone C., Evaluation of the Overall Crystalline Quality of Amorphous Carbon Containing Multi-Walled Carbon Nanotubes. *J. Phys. Chem. C.* **2013**, *117*, 4815−4823.

(20) Santangelo S.; Messina G.; Faggio G.; Abdul Rahim S.H.; Milone C., Effect of Sulphuric-Nitric Acid Mixture Composition on Surface Chemistry and Structural Evolution of Liquid-Phase Oxidised Carbon Nanotubes. *J. Raman Spectr.* **2012**, *43*, 1432−1442.

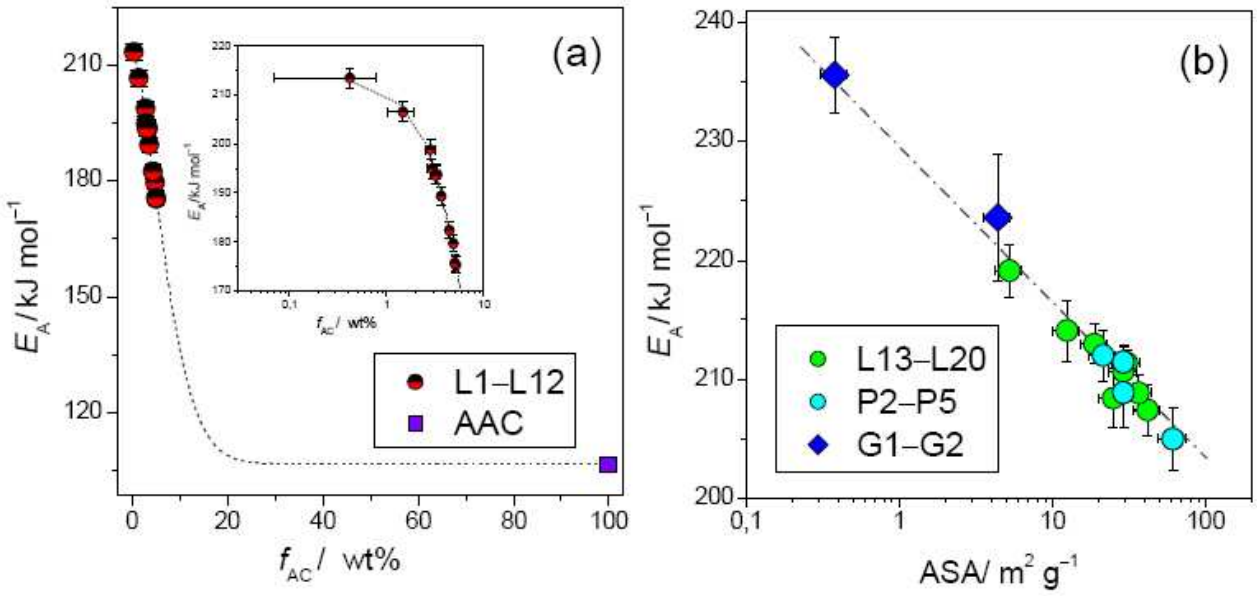

Figure S7. Dependence of the apparent activation energy (E_A) for the oxidation on (a) amorphous fraction of the sample (f_{AC}) as resulting from TG[15] in case of AAC and AC-containing MWNTs (see inset), and (b) active surface area (ASA) as estimated from Raman D/G integrated intensity ratio in case of AC-free MWNTs and crystalline graphite.